

Assessing the Predictive Value of Kolmogorov–Arnold Networks for the No-Reflow Phenomenon in ST-Segment Elevation Myocardial Infarction: A Comparative Machine Learning Study

ST Segment Yükselmeli Miyokard Enfarktüsünde No-Reflow Fenomeni için Kolmogorov–Arnold Ağlarının Öngörü Değerinin Değerlendirilmesi: Karşılaştırmalı Makine Öğrenimi Çalışması

ABSTRACT

Objective: The no-reflow phenomenon in ST-segment elevation myocardial infarction (STEMI) is a significant clinical issue associated with poor cardiovascular outcomes. This study aimed to develop and compare multiple supervised machine learning algorithms, including the recently introduced Kolmogorov–Arnold Network (KAN), to predict the occurrence of the no-reflow phenomenon in patients with STEMI undergoing primary percutaneous coronary intervention (PCI).

Method: This prospective, single-center study included 890 consecutive STEMI patients undergoing primary PCI. The Synthetic Minority Over-sampling Technique (SMOTE) was utilized to address class imbalance during training. Feature selection using analysis of variance (ANOVA) F-statistics and validation of feature independence (Variance Inflation Factor [VIF] < 5) identified ejection fraction (EF), baseline troponin level, stent length, B-type natriuretic peptide (BNP) level, and total ischemic time as the most influential predictors.

Results: The KAN and Extreme Gradient Boosting (XGBoost) models achieved the highest predictive accuracy (area under the curve > 0.98, F1 > 0.95), outperforming traditional models such as logistic regression and decision tree classifiers (DeLong test, $P < 0.001$). Feature selection improved efficiency and reduced runtime by 20–40%, while Shapley Additive exPlanations-based (SHAP-based) explainability confirmed that the predictions were physiologically consistent: higher EF and lower BNP reduced the probability of no-reflow, whereas longer stent length and ischemic time increased it. The superior performance of KAN and XGBoost underscores the importance of modeling nonlinear relationships and multidimensional interactions among clinical, laboratory, and procedural variables.

Conclusion: These findings suggest that KAN may serve as a reliable analytical framework for exploring complex cardiovascular outcomes. However, further multicenter and externally validated studies are needed to confirm its generalizability and potential role in clinical risk assessment.

Keywords: Extreme Gradient Boosting, Kolmogorov–Arnold network, machine learning, no-reflow phenomenon, Shapley Additive exPlanations explainability, ST-segment elevation myocardial infarction

ÖZET

Amaç: ST-segment yükselmeli miyokard enfarktüsünde (STEMI) görülen no-reflow fenomeni, kötü kardiyovasküler sonuçlarla ilişkilendirilen önemli bir klinik sorundur. Bu çalışma, primer perkütan koroner girişim (PKG) uygulanan STEMI hastalarında no-reflow fenomeninin görülmesini öngörmek amacıyla, yakın zamanda tanıtılan Kolmogorov–Arnold Ağı (KAN) da dâhil olmak üzere birden fazla denetimli makine öğrenimi algoritmasını geliştirmeyi ve karşılaştırmayı amaçlamıştır.

Yöntem: Bu ileriye dönük, tek merkezli çalışma, primer PKG uygulanan ardışık 890 STEMI hastasını kapsamıştır. Eğitim sırasında sınıf dengesizliğini gidermek amacıyla Sentetik Azınlık Aşırı Örnekleme Tekniği (SMOTE) kullanılmıştır. ANOVA F-istatistikleri kullanılarak yapılan özellik seçimi ve özellik bağımsızlığının doğrulanması (VIF < 5); ejeksiyon fraksiyonu (EF), bazal troponin seviyesi, stent uzunluğu, BNP seviyesi ve toplam iskemik süreyi en etkili öngörücüler olarak belirlemiştir.

ORIGINAL ARTICLE ARAŞTIRMA MAKALESİ

Hakan Taşolar¹

Adil Bayramoğlu¹

Mehmet Akif Günen²

Sümeyye Levent³

Yunus Güral³

Nurhan Halisdemir³

¹Department of Cardiology, İnönü University, Faculty of Medicine, Malatya, Türkiye

²Department of Geomatics Engineering, Gümüşhane University, Faculty of Engineering and Natural Sciences, Gümüşhane, Türkiye

³Department of Statistics, Fırat University, Faculty of Arts and Sciences, Elazığ, Türkiye

Corresponding author:

Hakan Taşolar
✉ hakantasolar@gmail.com

Received: October 16, 2025

Accepted: January 05, 2026

Cite this article as: Taşolar H, Bayramoğlu A, Günen MA, Levent S, Güral Y, Halisdemir N. Assessing the Predictive Value of Kolmogorov–Arnold Networks for the No-Reflow Phenomenon in ST-Segment Elevation Myocardial Infarction: A Comparative Machine Learning Study. *Türk Kardiyol Dern Ars.* 2026;54(3):236–244.

DOI: 10.5543/tkda.2026.02730



Copyright@Author(s)
Available online at archivestsc.com.
Content of this journal is licensed under a Creative Commons Attribution – NonCommercial–NoDerivatives 4.0 International License.

Bulgular: KAN ve XGBoost modelleri, en yüksek tahmin doğruluğuna ulaşarak (AUC > 0,98, F1 > 0,95), lojistik regresyon ve karar ağacı sınıflandırıcıları gibi geleneksel modelleri istatistiksel olarak anlamlı düzeyde geride bırakmıştır (P < 0,001). Özellik seçimi, verimliliği artırmış ve çalışma süresini %20–40 oranında azaltmıştır; SHAP tabanlı açıklanabilirlik ise tahminlerin fizyolojik olarak tutarlı olduğunu doğrulamıştır. Daha yüksek EF ve daha düşük BNP, no-reflow olasılığını azaltırken; daha uzun stent uzunluğu ve iskemik süre bu olasılığı artırmıştır. KAN ve XGBoost'un üstün performansı, klinik, laboratuvar ve prosedürel değişkenler arasındaki doğrusal olmayan ilişkilerin ve çok boyutlu etkileşimlerin modellenmesinin önemini vurgulamaktadır.

Sonuç: Bu bulgular, KAN'ın karmaşık kardiyovasküler sonuçların incelenmesinde güvenilir bir analitik çerçeve olarak hizmet edebileceğini göstermektedir. Ancak, genellebilirliğinin ve klinik risk değerlendirmesindeki potansiyel rolünün doğrulanması için çok merkezli ve harici olarak doğrulanmış ek çalışmalara ihtiyaç vardır.

Anahtar Kelimeler: Aşırı Gradyan Güçlendirme, Kolmogorov–Arnold ağı, makine öğrenimi, no-reflow fenomeni, Shapley Additive exPlanations açıklanabilirlik, ST-segment yükselmeli miyokard enfarktüsü

The no-reflow phenomenon in ST-segment elevation myocardial infarction (STEMI) is a significant clinical issue that can hinder recovery, even after successful primary percutaneous coronary intervention (PCI). It is characterized by inadequate myocardial tissue perfusion despite reopening of the infarct-related coronary artery. Various studies have explored the mechanisms, predictors, and consequences of this phenomenon, as well as how machine learning (ML) can aid in its prediction and management. The no-reflow phenomenon is associated with poor cardiovascular outcomes in patients with STEMI and may present as an in-hospital complication, including arrhythmias and cardiogenic shock.^{1,2} The pathophysiology involves multiple factors, including endothelial dysfunction, microvascular spasm, distal embolization, and reperfusion injury.¹

The pathophysiology of the no-reflow phenomenon is complex and multifactorial, primarily involving ischemic injury followed by reperfusion injury. This process leads to oxidative stress, intracellular calcium overload, and an intense inflammatory response.^{1,2} Key mechanisms contributing to microvascular obstruction include distal embolization of atherosclerotic debris or thrombus, endothelial swelling, and accumulation of neutrophils and platelets that physically obstruct the microcirculation. These pathological changes prevent effective myocardial perfusion at the tissue level, even when the epicardial coronary artery is successfully recanalized.²

In recent years, several biochemical and hematological indices have been proposed to improve risk stratification for the no-reflow phenomenon in patients with STEMI. These indices integrate inflammatory, lipid-related, and metabolic parameters, offering a more comprehensive assessment compared to conventional clinical predictors.^{3–6}

In the context of predicting the no-reflow phenomenon, ML models have been increasingly applied across various fields owing to their predictive accuracy and ability to analyze large datasets. Although the specific application of ML models to the no-reflow phenomenon, commonly associated with coronary interventions, has not been directly addressed in the retrieved literature, several related ML approaches are commonly used in medical predictive tasks and can be extrapolated to no-reflow prediction.

ABBREVIATIONS

ANN	Artificial Neural Networks
ANOVA	Analysis of variance
BNP	B-type natriuretic peptide
CABG	Coronary artery bypass grafting
CK-MB	Creatine kinase–myocardial band
EF	Ejection fraction
KAN	Kolmogorov–Arnold Network
MBG	Myocardial Blush Grade
ML	Machine learning
PCI	Percutaneous coronary intervention
RF	Random Forest
SMOTE	Synthetic Minority Over-sampling Technique
STEMI	ST-segment elevation myocardial infarction
SVM	Support Vector Machines
SYNTAX	Synergy Between Percutaneous Coronary Intervention with TAXUS and Cardiac Surgery
TIMI	Thrombolysis in Myocardial Infarction
VIF	Variance Inflation Factor

In cardiovascular and medical applications, ML models such as Support Vector Machines (SVM), Artificial Neural Networks (ANN), and ensemble methods, including Random Forest (RF) and Gradient Boosting, have been frequently employed owing to their proficiency in classification and prediction tasks.^{7,8} These models are known for their ability to handle complex interactions within data, making them suitable for predicting clinical outcomes such as no-reflow, which involves multifactorial influences.

This study aimed to develop and compare multiple supervised machine learning algorithms, including the recently introduced Kolmogorov–Arnold Network (KAN), to predict the occurrence of the no-reflow phenomenon in patients with STEMI undergoing primary PCI. By integrating comprehensive clinical, laboratory, and angiographic parameters, this study sought to evaluate the predictive performance, interpretability, and computational efficiency of KAN in comparison with conventional models such as Extreme Gradient Boosting (XGBoost), Multilayer Perceptron (MLP), and logistic regression, and to determine whether feature selection and model explainability could enhance risk stratification and clinical interpretability in real-world STEMI cohorts.

Materials and Methods

Patient Selection and Data Source

This prospective, single-center investigation included 890 consecutive patients who presented to our institution's emergency department between 2022 and 2024 with a confirmed diagnosis of STEMI. Each patient underwent primary PCI within 15 hours of the onset of chest pain. The criteria for diagnosing STEMI included chest pain or an angina equivalent lasting more than 30 minutes, ST-segment elevation of at least 1 mm in two or more contiguous leads, and a subsequent increase in creatine kinase (CK), creatine kinase-myocardial band (CK-MB), or troponin levels following PCI. The study was approved by the İnönü University Scientific Research and Publication Ethics Committee (Approval Number: 2022/3133, Date: 08.03.2022), and adhered to the Declaration of Helsinki and Good Clinical Practice guidelines. Written informed consent was obtained from all participants before inclusion in the study.

The detailed clinical, echocardiographic, and angiographic definitions—including criteria for Thrombolysis in Myocardial Infarction (TIMI) flow grading, thrombus burden, Killip class, and SYNTAX (Synergy Between Percutaneous Coronary Intervention With TAXUS and Cardiac Surgery) score assessment—were previously described in our earlier publication.⁹ Specifically, the no-reflow phenomenon was defined angiographically as a TIMI flow grade < 3, or a TIMI flow grade of 3 with a Myocardial Blush Grade (MBG) < 2 in the absence of mechanical obstruction, dissection, or distal macroembolism immediately following the procedure. In the current study, the same inclusion and exclusion criteria were applied, and all definitions of demographic and procedural variables were kept consistent with the prior methodology to ensure data comparability.

Data Collection and Variable Description

A total of 37 demographic, clinical, laboratory, and angiographic features were initially included in the dataset. These variables included left ventricular ejection fraction (EF), stent length and diameter, total ischemic time, TIMI thrombus score, SYNTAX score, cardiac biomarkers (troponin, brain natriuretic peptide (BNP), and C-reactive protein [CRP]), and baseline hemodynamic and metabolic parameters such as blood pressure, hemoglobin, lipid profile, and inflammatory indices.

To identify the most informative predictors, feature importance ranking was conducted using one-way analysis of variance (ANOVA) F-statistics. These parameters were prioritized for subsequent modeling analyses. To ensure the absence of multicollinearity, a Variance Inflation Factor (VIF) analysis was performed. All VIF values were < 5, indicating acceptable feature independence.

Prior to model training, a comprehensive data quality check was performed. The distributions of the 37 baseline demographic, clinical, and angiographic variables are presented in Table 1. Missing data were handled using K-Nearest Neighbors (KNN) imputation, which estimates missing values based on the similarity of multidimensional feature vectors, thereby preserving dataset integrity without sample loss. Subsequently, to address class imbalance within this cohort (lower incidence of no-reflow), the Synthetic Minority Over-sampling Technique (SMOTE) was applied exclusively to the training folds during the cross-validation process.

Table 1. Baseline demographic, clinical, and angiographic characteristics

Variables	n = 890
Demographic data	
Age	58.1 ± 12.2
Male sex	737 (82.8%)
Smoking	502 (56.4%)
Diabetes mellitus	201 (22.6%)
Hypertension	403 (45.3%)
Dyslipidemia	371 (41.7%)
Family history	193 (21.7%)
Clinical data	
History of MI	84 (9.4%)
History of PCI	89 (10.0%)
History of CABG	22 (2.5%)
Hemodialysis	0 (0.0%)
ASA	101 (11.3%)
Beta-blocker use	118 (13.3%)
Statin use	182 (20.4%)
Killip class	
I	818 (91.9%)
II	60 (6.7%)
III	4 (0.4%)
IV	8 (0.9%)
Pre-angina score	210 (23.6%)
Angiographic and procedural data	
Tirofiban (bolus)	430 (48.3%)
SYNTAX score	15.2 ± 7.0
CTO	28 (3.1%)
Lesion localization	
Proximal	470 (52.8%)
Mid	376 (42.2%)
Distal	44 (4.9%)
Infarct-related artery	
LAD	469 (52.7%)
CX	134 (15.1%)
RCA	269 (30.2%)
Saphenous graft	4 (0.4%)
Other	14 (1.6%)
Number of diseased vessels	
One-vessel disease	569 (63.9%)
Two-vessel disease	209 (23.5%)
Three-vessel disease	112 (12.6%)
TIMI thrombus score	4.4 ± 0.9
Stent length	21.3 ± 8.8
Stent diameter	3.1 ± 0.3
Direct stenting	258 (29.0%)
Total ischemic time	200.6 ± 108.4
Door-to-balloon time	29.7 ± 5.8
Corrected TFC	24.1 ± 14.1

ASA, Acetylsalicylic acid; CABG, Coronary artery bypass grafting; CTO, Chronic total occlusion; MI, Myocardial infarction; PCI, Percutaneous coronary intervention; TFC, TIMI frame count; TIMI, Thrombolysis in myocardial infarction.

Feature Selection Strategy

The feature selection process was designed to enhance model efficiency and generalizability by identifying the most informative predictors among all candidate variables. The workflow consisted of two sequential stages. Initially, a full-feature modeling approach was employed, incorporating all 37 demographic, laboratory, and angiographic variables to establish a baseline reference model. In the subsequent stage, a reduced-feature modeling approach was implemented, retaining only the top-ranked variables as determined by ANOVA F-statistics and verified for low multicollinearity through VIF analysis. This two-step strategy facilitates assessment of whether dimensionality reduction enhances model stability, mitigates the risk of overfitting, and improves the generalizability of machine learning algorithms without compromising predictive accuracy.

Machine Learning Framework

To predict the occurrence of the no-reflow phenomenon, six supervised machine-learning algorithms with distinct architectures were developed and evaluated. The Decision Tree (C4.5) algorithm was used as a rule-based classifier to segment data into homogeneous groups through recursive partitioning.¹⁰ The K-Nearest Neighbors algorithm classified patients based on feature similarity using distance metrics in multidimensional space. Logistic Regression (LR) provided a benchmark linear model for estimating event probability from weighted predictors.¹¹ The XGBoost algorithm, a tree-based ensemble learning method, was employed to capture nonlinear feature interactions using gradient-based optimization and regularization.¹² The MLP, a feedforward neural network trained by backpropagation, was applied to model complex nonlinear relationships between clinical and angiographic data.¹³ Finally, the KAN, a recent spline-based deep learning framework, was implemented according to its original formulation.¹⁴

These algorithms were selected to reflect the complex and multifaceted clinical structure of the no-reflow phenomenon. This diversity aimed to identify the most suitable strategy for predicting no-reflow by enabling a comprehensive comparison of both model architectures and learning paradigms. In this study, machine learning models were evaluated using Python. For model implementation, the scikit-learn library (Decision Tree, KNN, Logistic Regression), XGBoost library (XGBoost), PyTorch frameworks, MLP, and pykan library (KAN) were used.

Performance Evaluation

Model performance was assessed using a set of standard classification metrics to ensure a comprehensive evaluation of predictive ability. The following measures were calculated for each model: accuracy, precision, recall, F1-score, and area under the receiver operating characteristic curve (AUC). These metrics collectively quantify the discrimination capacity of the models, the balance between sensitivity and specificity, and overall classification consistency.

In addition, runtime (s) was recorded for each algorithm to evaluate computational efficiency. Receiver operating characteristic (ROC) curves were generated to visualize model discrimination before and after feature selection.

The dataset was split into 70% training and 30% test sets using a stratified hold-out method to objectively evaluate model generalization performance. Five-fold cross-validation was applied to the training data for hyperparameter optimization (Grid Search) and for internal performance assessment of the models. During this process, cross-validation was performed exclusively on the training set. For model selection and evaluation, external validity and the risk of overfitting were minimized using an independent 30% test dataset that the model had never seen before. The reported performance metrics were obtained from the test set to reflect predictive ability of the model under real-world conditions. Performance evaluation and cross-validation procedures were performed using libraries such as Python scikit-learn and imbalanced-learn.

Explainability Analysis

To enhance model transparency and interpretability, SHapley Additive exPlanations (SHAP) analysis was applied to the final trained models. This approach decomposes individual predictions into additive feature contributions, enabling both global and local interpretation of model outputs. SHAP summary plots were generated to illustrate the overall importance and directionality of each variable's influence on prediction outcomes, while SHAP waterfall plots were used to visualize case-specific feature impacts and cumulative contribution patterns.^{15,16} Global and local explainability analyses were conducted to enhance model interpretability using the Python SHAP library. The matplotlib and seaborn libraries were used for visualization.

Statistical Analysis and Software

Continuous variables were expressed as mean \pm standard deviation (SD) and compared using Student's t-test or the Mann-Whitney U test, depending on data distribution. Categorical variables were presented as percentages and analyzed using the chi-square test or Fisher's exact test, where appropriate. A p-value < 0.05 was considered statistically significant.

All machine learning models were developed and executed in Python (v3.12). Hyperparameter optimization was performed using grid search with algorithm-specific tuning of learning rate, network depth, and regularization parameters. Model training was designed to maximize the F1-score and AUC while minimizing computational runtime to achieve optimal performance. Model interpretability was assessed using the SHAP library integrated into Python, ensuring consistent post hoc explainability across all algorithms. Descriptive and inferential statistical analyses were conducted using SPSS version 26.0 (IBM Corp., Armonk, NY, USA), whereas visualization and performance metrics were generated using the matplotlib and SHAP packages in Python.

Results

Baseline Demographic, Clinical, and Angiographic Characteristics

This study included 890 patients diagnosed with STEMI. The average age of these individuals was 58.1 ± 12.2 years. There was a significant prevalence of traditional cardiovascular risk factors among participants, with smoking (56.4%), hypertension (45.3%), dyslipidemia (41.7%), and diabetes mellitus (22.6%) being the most common. Additionally, 21.7% of patients had a family history of coronary artery disease. In terms of pre-admission medical therapy, 11.3% of patients were administered

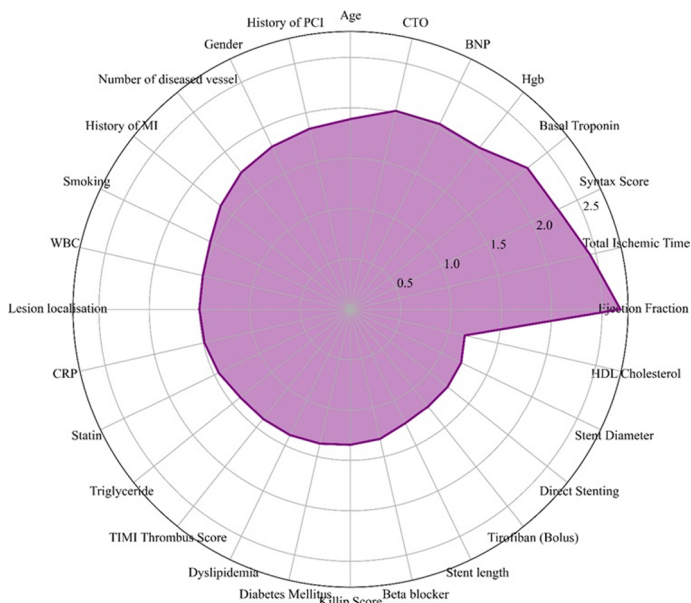


Figure 1. Variance Inflation Factor (VIF) analysis of selected features. This radar chart visualizes the VIF values for the candidate predictor variables. The radial axes represent individual clinical and angiographic features, while the concentric circles indicate VIF thresholds. The purple shaded area demonstrates that all variables have VIF values well below the critical threshold of 5, confirming the absence of significant multicollinearity and ensuring the independence of the features used in the modeling process.

acetylsalicylic acid, 13.3% were prescribed beta-blockers, and 20.4% received statin therapy. Prior cardiovascular interventions were relatively infrequent, with 9.4% of patients having a history of myocardial infarction, 10.0% having undergone PCI, and 2.5% having undergone coronary artery bypass grafting (CABG). None of the patients underwent chronic hemodialysis.

Angiographic and procedural parameters showed a mean SYNTAX score of 15.2 ± 7.0 and a mean TIMI thrombus score of 4.4 ± 0.9 . Chronic total occlusion was observed in 3.1% of cases, whereas direct stenting was performed in 29.0% of cases. The mean stent length was 21.3 ± 8.8 mm, with an average stent diameter of 3.1 ± 0.3 mm. The mean total ischemic time was 200.6 ± 108.4 minutes, and the mean door-to-balloon time was 29.7 ± 5.8 minutes, indicating prompt revascularization. The corrected TIMI frame count (TFC) was 24.1 ± 14.1 , consistent with the angiographic findings presented in Table 1.

Feature Selection and Model Performance

Feature importance analysis using ANOVA F-statistics identified variables associated with ventricular function, ischemic duration, and angiographic complexity as the most discriminative predictors of the no-reflow phenomenon (Table 2). The highest-ranking features included EF, baseline troponin level, stent length, BNP level, and total ischemic time, reflecting the combined influence of myocardial function and procedural parameters.

To evaluate potential interdependence among the selected predictors, a VIF analysis was performed. As shown in Figure 1, all variables demonstrated VIF values below 5, confirming the

Table 2. Feature importance scores based on ANOVA F-statistics

Ejection fraction	39.6127
Baseline troponin	33.3236
Stent length	32.9244
BNP	28.9555
Total ischemic time	22.2068
CTO	20.575
SYNTAX score	15.0598
CRP	13.9356
Age	11.7462
Direct stenting	10.3063
Stent diameter	9.1559
Statin use	8.2875
Killip class	7.6746
Lesion localization	7.3628
TIMI thrombus score	6.7071
Hgb	5.466
WBC	5.1448
Smoking	4.0696
Number of diseased vessels	3.6549
Diabetes mellitus	3.3704
Tirofiban (bolus)	2.2916
Sex	1.7781
Beta-blocker use	1.7555
History of MI	1.5564
Dyslipidemia	1.4562
Triglycerides	1.2415
History of PCI	1.1027
HDL cholesterol	1.0034
Pre-angina score	0.7585
History of CABG	0.6592
ASA use	0.5223
Infarct-related artery	0.3551
Hypertension	0.1003
Door-to-balloon time	0.0785
LDL cholesterol	0.0575
Heart rate	0.0491
Systolic blood pressure	0.0069
Hemodialysis	0

ASA, Acetylsalicylic acid; BNP, B-type natriuretic peptide; CABG, Coronary artery bypass grafting; CRP, C-reactive protein; CTO, Chronic total occlusion; HDL, High-density lipoprotein; Hgb, Hemoglobin; LDL, Low-density lipoprotein; MI, Myocardial infarction; PCI, Percutaneous coronary intervention; SYNTAX, Synergy between percutaneous coronary intervention with TAXUS and cardiac surgery; TFC, TIMI frame count; TIMI, Thrombolysis in myocardial infarction; WBC, White blood cell count.

absence of multicollinearity. This finding indicates that each feature contributes unique information to the model without redundancy, thereby supporting the stability and interpretability of the final predictive framework.

Table 3. Performance comparison of models before and after feature selection

Model	Accuracy	Precision	Recall	F1-Score	ROC AUC	Runtime (s)
Decision tree	90.82/91.22	91.02/90.12	90.65/92.68	90.84/91.38	90.82/91.22	0.041/0.026
KNN	89.39/80	84.64/72.56	96.34/96.75	90.11/82.93	97.53/94.72	0.052/0.050
Logistic regression	83.47/84.9	84.23/85.83	82.52/83.74	83.37/84.77	91.67/92.57	0.021/0.022
XGBoost	94.49/95.1	95.06/95.49	93.9/94.72	94.48/95.1	98.28/98.37	0.052/0.043
MLP	85.31/81.84	85.08/79.62	85.77/85.77	85.43/82.58	90.9/89.02	0.170/0.174
KAN	92.04/94.49	94.87/96.27	90.24/94.31	92.5/95.28	98.46/98.19	22.22/20.81

KAN, Kolmogorov–Arnold Network; KNN, K-Nearest Neighbors; MLP, Multilayer Perceptron; ROC AUC, Receiver Operating Characteristic – Area Under the Curve; XGBoost, Extreme Gradient Boosting.

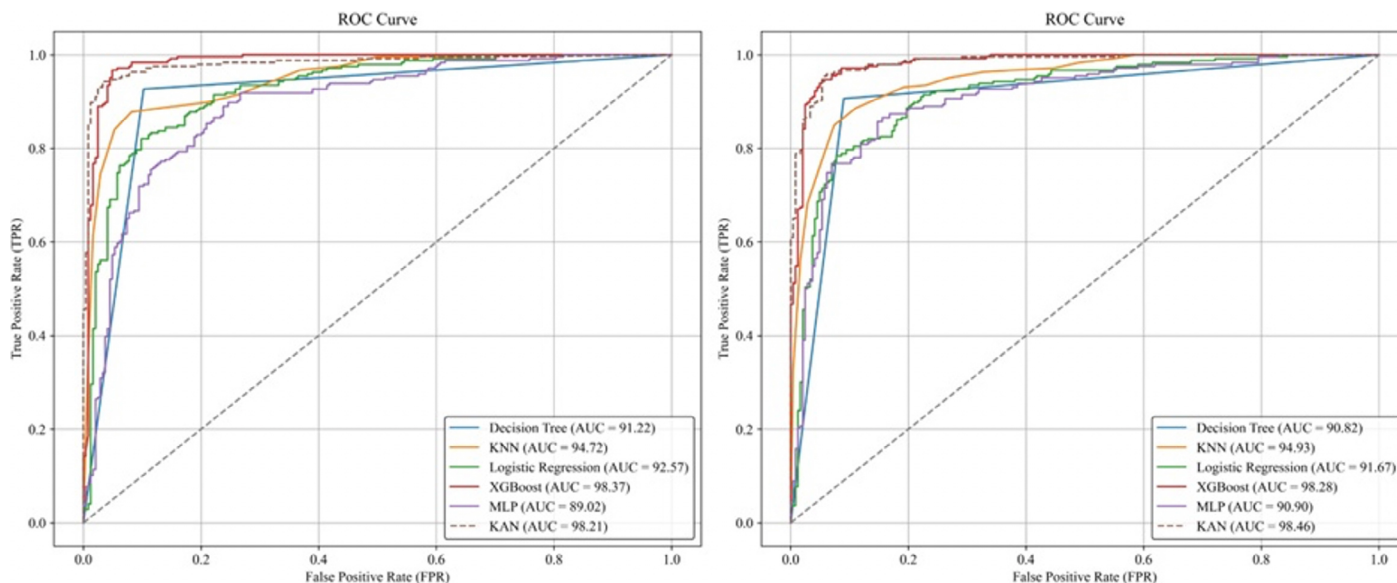


Figure 2. Receiver Operating Characteristic (ROC) curve comparison before and after feature selection. The panels display the ROC curves for the six machine learning algorithms evaluated. The left panel illustrates model performance using the full set of variables, whereas the right panel shows performance after applying feature selection. The x-axis represents the False Positive Rate (1 - specificity) and the y-axis represents the True Positive Rate (sensitivity). The Kolmogorov–Arnold Network (KAN) model (dashed brown line) and Extreme Gradient Boosting (XGBoost) model (red line) exhibit the largest Area Under the Curve (AUC), indicating superior discriminative ability in predicting the no-reflow phenomenon compared to traditional models such as logistic regression and decision trees.

After applying feature selection, the performance of all machine learning models was re-evaluated. As shown in Table 3, dimensionality reduction improved overall model stability and computational efficiency. Among the algorithms, XGBoost and KAN demonstrated the highest predictive performance, achieving AUC values above 0.98 and F1-scores exceeding 0.95. These models effectively captured nonlinear and hierarchical relationships within the dataset, outperforming traditional classifiers such as logistic regression and decision tree models.

The results also indicated that feature selection enhanced accuracy and reduced runtime by approximately 20–40% across all algorithms, suggesting that eliminating redundant or low-impact variables improved both computational feasibility and generalizability. Although the KAN model required longer processing time owing to its spline-based nonlinear structure, it provided superior interpretability and a balanced trade-off between precision and efficiency.

Overall, the combination of feature selection and advanced learning architectures such as KAN and XGBoost yielded the most reliable and clinically meaningful predictions of the no-reflow phenomenon in patients with STEMI.

Receiver Operating Characteristic Analysis

Figure 2 illustrates the ROC curves of all machine learning models before and after feature selection. The overall shape of the post-selection ROC curves shifted toward the upper-left corner of the plot, indicating a clear improvement in discriminative performance. The AUC increased across all algorithms, demonstrating that the elimination of redundant variables enhanced the ability of the models to distinguish between patients with and without no-reflow.

The ROC profiles also became smoother after dimensionality reduction, suggesting greater model stability and reduced variability across cross-validation folds. Among the algorithms, ensemble and neural models, particularly XGBoost and KAN,

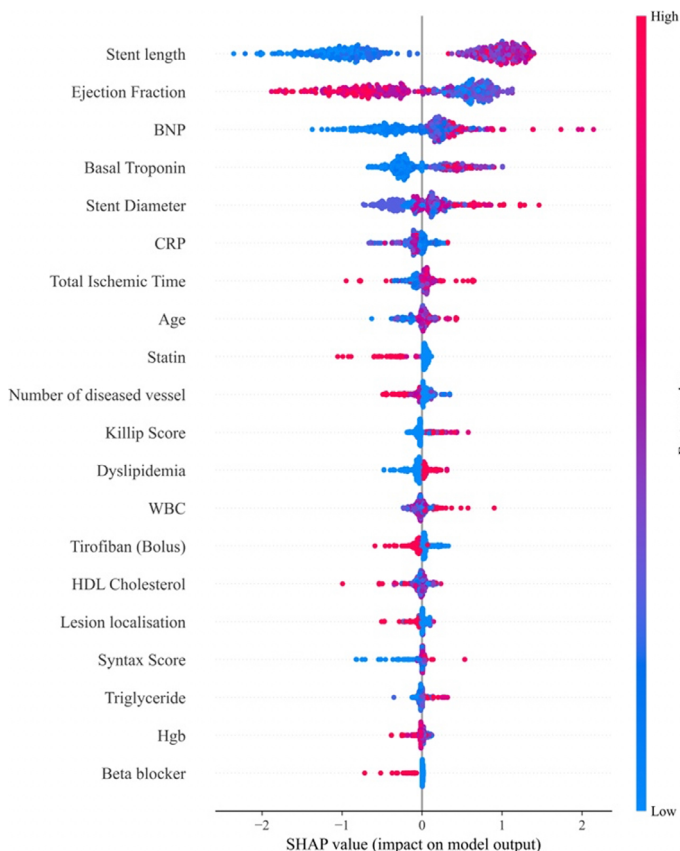


Figure 3. Shapley Additive exPlanations (SHAP) summary plot for selected features. This plot illustrates the global importance and impact of clinical features on the prediction of the no-reflow phenomenon using the model. Features are ranked on the y-axis in descending order of importance, with stent length and ejection fraction being the most influential. Each dot represents an individual patient. Color indicates the feature value (red = high value, blue = low value). The position on the x-axis (SHAP value) reflects the direction of impact: points to the right (positive values) increase the probability of no-reflow, whereas points to the left (negative values) decrease it. For example, higher stent length (red dots) is associated with positive SHAP values, indicating increased risk.

displayed the steepest initial ascent and largest enclosed area, confirming their superior classification performance compared to conventional methods.

To verify the statistical significance of these performance differences, DeLong's test was applied to the ROC curves. The analysis revealed that while the performance difference between KAN and XGBoost was not statistically significant ($P > 0.05$), both KAN and XGBoost demonstrated statistically significant improvements in discriminative ability compared to logistic regression and decision tree classifiers ($P < 0.001$), confirming the superiority of nonlinear modeling approaches.

Explainability and Feature Contribution Analysis

To enhance the clinical interpretability of the predictive models, SHAP analysis was used to identify how each variable influenced the model's decisions. Rather than focusing on mathematical details, SHAP outputs were interpreted in a clinically meaningful manner.

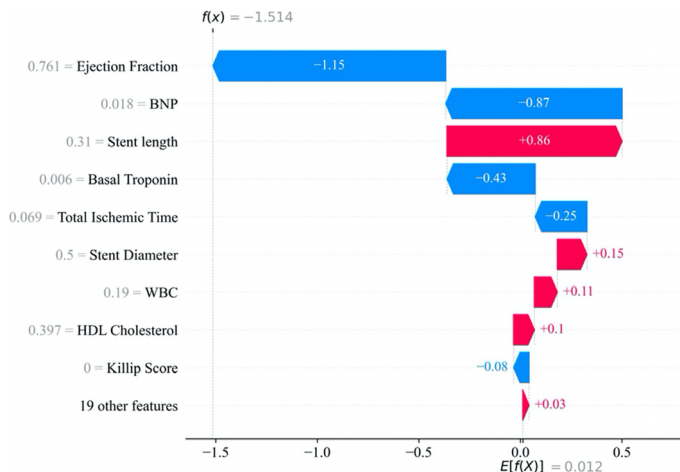


Figure 4. Shapley Additive exPlanations (SHAP) waterfall plot for a representative case. This plot illustrates the contribution of individual features to the prediction score $f(x)$ for a specific patient. The base value ($E[f(X)]$) represents the average model output across the dataset. Red bars indicate features that push the prediction toward the no-reflow outcome (increasing risk), such as stent length, while blue bars indicate features that push the prediction toward normal flow (decreasing risk), such as higher ejection fraction. In this example, the strong protective effect of functional parameters (blue bars) outweighs procedural risk factors, resulting in a negative final score $f(x) = -1.514$, corresponding to a low probability of no-reflow.

The SHAP summary plot demonstrates that variables reflecting myocardial function (ejection fraction and BNP), ischemic burden (total ischemic time and baseline troponin), and procedural complexity (stent length) were the dominant contributors to prediction of the no-reflow phenomenon. Higher ejection fraction and lower BNP levels consistently decreased the predicted risk of no-reflow, whereas longer stent length and prolonged ischemic time increased the predicted risk (Figure 3).

The SHAP waterfall plot enabled patient-level interpretation by illustrating how individual clinical factors shifted the prediction toward higher or lower risk. In the representative case, preserved ejection fraction and low BNP exerted a strong protective effect, whereas longer stent length increased risk. These findings demonstrate that the model's predictions rely on clinically established pathophysiological mechanisms rather than spurious correlations (Figure 4).

Accordingly, SHAP analysis was used as a transparent clinical explanation tool rather than a purely technical mathematical framework.

Discussion

In this study, multiple machine learning algorithms were compared to predict the no-reflow phenomenon in patients with STEMI undergoing primary PCI. After feature selection using ANOVA F-statistics and validation of feature independence ($VIF < 5$), the most influential predictors were EF, baseline troponin level, stent length, BNP level, and total ischemic time. Model comparison revealed that KAN and XGBoost achieved the highest

predictive accuracy (AUC > 0.98, F1 > 0.95), outperforming traditional models such as logistic regression and decision tree classifiers. Feature selection improved efficiency and reduced runtime by 20–40%, while SHAP-based explainability confirmed that the predictions were physiologically consistent: higher EF and lower BNP reduced the probability of no-reflow, whereas longer stent length and ischemic time increased it.

Coronary no-reflow is characterized by inadequate myocardial reperfusion after reopening the infarct-related artery during primary percutaneous coronary intervention and accounts for up to 40% of cases with incomplete myocardial reperfusion despite restored artery patency. The pathophysiology involves microvascular obstruction and is associated with increased mortality, arrhythmias, and heart failure. Diagnostic approaches include angiographic scoring and advanced imaging techniques such as myocardial contrast echocardiography and cardiac magnetic resonance imaging. Prevention and treatment strategies incorporate both pharmacological therapies and device-based interventions.¹ ML has been applied in cardiology, including coronary artery disease and cardiac imaging, with promising results. ML algorithms can analyze large datasets to enable earlier diagnosis, improved risk stratification, and individualized therapy. In coronary artery disease, ML supports cardiac imaging through score computation, phenotypic differentiation, heart function quantification, and segmentation, thereby enhancing anomaly detection and cardiovascular risk prediction.¹⁷ While direct studies on coronary no-reflow prediction using ML algorithms are limited, clinical predictors—such as admission hyperglycemia, reperfusion delay, thrombus burden, and blood biomarkers—serve as crucial input features for ML models aimed at risk stratification in acute coronary syndromes (ACS), where no-reflow commonly manifests.^{18–20}

Supervised machine learning algorithms have shown promise in predicting coronary events, including the no-reflow phenomenon. For cardiovascular prediction tasks, LR, SVM, Naïve Bayes, KNN, RF, and XGBoost are among the most widely evaluated models¹⁴. Logistic regression and gradient boosting techniques, particularly XGBoost, have demonstrated superior performance in clinical outcome prediction, achieving acceptable to high AUC values in cardiac surgery mortality and cardiovascular endpoints.^{21,22} Khalaji et al.²¹ evaluated multiple ML algorithms for mortality prediction after coronary artery bypass grafting and demonstrated the superiority of ensemble learning models over conventional approaches. Our study showed that XGBoost and KAN significantly outperformed logistic regression and decision tree models. Kendale et al.²² reported that gradient-based learning models provide high predictive accuracy for post-induction hypotension in cardiovascular patients, supporting the use of boosting-based methods in acute care settings. The high performance of XGBoost in our study directly parallels these observations.

Deng et al.²³ reported moderate success using a random forest model to predict no-reflow and mortality in STEMI patients undergoing primary PCI. In contrast, our KAN and XGBoost models performed better, demonstrating the superiority of advanced learning methods in understanding microvascular reperfusion failure. While Celik et al.²⁴ found the red cell distribution width-to-platelet ratio to be a predictor of no-reflow, our model identified heart function

and procedural complexity as more significant predictors. Similarly, Wang et al.²⁰ identified inflammatory and biochemical parameters as predictors of the no-reflow phenomenon. Our model confirmed baseline troponin and BNP as strong predictors of the no-reflow condition. Dong-Bao et al.¹⁹ linked prolonged ischemic time and thrombus burden to slow/no-reflow, and in our study, total ischemic time and stent length emerged as top predictors. While Celik et al.³ emphasized blood count parameters, our cohort demonstrated functional and procedural factors such as ejection fraction, BNP, and stent length were dominant, suggesting that mechanical factors outweigh inflammation. Although Kurtul et al.²⁵ and Toprak et al.²⁶ highlighted inflammatory markers, our findings indicate that physical and blood flow-related factors play a more significant role.

The study also identified that higher ejection fraction and lower levels of B-type natriuretic peptide were associated with a reduced risk of the no-reflow phenomenon, indicating that optimal cardiac function facilitates effective blood circulation. Conversely, the use of longer stents may increase the risk of no-reflow due to potential damage to smaller blood vessels. Additionally, prolonged ischemic duration was associated with increased risk, underscoring the detrimental effects of interrupted blood flow. These findings are consistent with established etiologies of the no-reflow phenomenon. Stent length and the time without blood flow highlight the need to address blockage in small blood vessels. Low EF and elevated BNP levels illustrate how impaired blood flow affects small vessels. This helps identify high-risk patients early, especially those needing long stents or experiencing long periods without blood flow, suggesting that additional treatments might be needed. Our model uses different factors to predict no-reflow in patients with STEMI. Unlike past studies that focused on single markers or simple models, our research includes heart function, blood markers, stent length, and time without blood flow in a detailed deep learning model. This improves the prediction of no-reflow and shows how artificial intelligence can help manage STEMI cases.

There are concerns that the high AUC and F1-scores might indicate that the model is overfitting. To address this, a careful method was used. The model was trained on 70% of the data, and its settings were fine-tuned using five-fold cross-validation only on this portion. This prevented any data from leaking into the test phase. The final results came from the remaining 30% of the data, which the model had not seen before. The high accuracy likely reflects a strong link between the key features—EF, BNP, and total ischemic time—and the no-reflow phenomenon rather than overfitting. However, we acknowledge that the lack of external validation and a full calibration analysis is a limitation, meaning that the high scores should be interpreted with caution.

This study was conducted using a single-center prospective design, which inherently limits the generalizability of our findings to a broader patient population. The absence of external validation restricts the confidence with which these results can be extrapolated to other institutions with different demographic profiles or procedural protocols. Consequently, while the KAN model demonstrates high internal validity, rigorous testing in diverse multicenter cohorts is essential to confirm its robustness and ensure that the reported predictive accuracy is reproducible in real-world clinical settings.

Conclusion

This study demonstrates that Kolmogorov–Arnold Networks provide highly accurate prediction of the no-reflow phenomenon in patients with STEMI. However, the model requires external multicenter validation before any clinical implementation. At present, KAN should be considered a promising research tool rather than a ready-to-use clinical decision support system.

Ethics Committee Approval: Ethics committee approval was obtained from İnönü University Scientific Research and Publication Ethics Committee (Approval Number: 2022/3133, Date: 08.03.2022).

Informed Consent: Written informed consent was obtained from all participants before inclusion in the study.

Conflict of Interest: The authors have no conflicts of interest to declare.

Funding: The authors declared that this study received no financial support.

Use of AI for Writing Assistance: No artificial intelligence (AI)-assisted technologies, including large language models (LLMs), chatbots, or image generators, were used in the writing, data analysis, figure preparation, or any other aspect of the production of this manuscript.

Author Contributions: Concept – H.T., A.B., M.A.G., S.L., Y.G., N.H.; Design – H.T., A.B., M.A.G.; Supervision – H.T., M.A.G., S.L., Y.G., N.H.; Resource – H.T., A.B.; Materials – H.T., A.B.; Data Collection and/or Processing – H.T., A.B., M.A.G.; Analysis and/or Interpretation – H.T., M.A.G., S.L., Y.G., N.H.; Literature Review – H.T., A.B., M.A.G.; Writing – H.T., A.B., M.A.G., S.L., Y.G., N.H.; Critical Review – H.T., M.A.G.

Peer-review: Externally peer-reviewed.

References

1. Yılmaz C, Ünğan İ, Arslan E, et al. The HALP Score's Prognostic Value for the Elderly Patients (≥ 75 years) Patients Following Percutaneous Coronary Intervention for Acute Myocardial Infarction. *Turk Kardiyol Dern Ars.* 2025;53(6):388–397. [CrossRef]
2. Pantea-Roşan LR, Pantea VA, Bungau S, et al. No–Reflow after PPCI–A Predictor of Short–Term Outcomes in STEMI Patients. *J Clin Med.* 2020;9(9):2956. [CrossRef]
3. Celik T, Balta S, Mikhailidis DP, et al. The Relation Between No–Reflow Phenomenon and Complete Blood Count Parameters. *Angiology.* 2017;68(5):381–388. [CrossRef]
4. Özbay MB, Değirmen S, Güllü A, Nriagu BN, Özen Y, Yayla Ç. Association of the C–Reactive Protein to Albumin Ratio with the No–Reflow Phenomenon After Percutaneous Coronary Intervention: A Systematic Review and Meta–Analysis. *Turk Kardiyol Dern Ars.* 2025;53(6):428–432. [CrossRef]
5. Vatan MB, Çakmak AC, Ağaç S, Eynel E, Erkan H. The Systemic Immune–Inflammation Index Predicts Impaired Myocardial Perfusion and Short–Term Mortality in ST–Segment Elevation Myocardial Infarction Patients. *Angiology.* 2023;74(4):365–373. [CrossRef]
6. Süleymanoğlu M, Rencüzoğulları İ, Karabağ Y, et al. The relationship between atherogenic index of plasma and no-reflow in patients with acute ST–segment elevation myocardial infarction who underwent primary percutaneous coronary intervention. *Int J Cardiovasc Imaging.* 2020;36(5):789–796. [CrossRef]
7. Cuocolo R, Perillo T, De Rosa E, Ugga L, Petretta M. Current applications of big data and machine learning in cardiology. *J Geriatr Cardiol.* 2019;16(8):601–607.
8. Battineni G, Sagaro GG, Chinatalapudi N, Amenta F. Applications of Machine Learning Predictive Models in the Chronic Disease Diagnosis. *J Pers Med.* 2020;10(2):21. [CrossRef]
9. Bayramoğlu A, Taşolar H, Kaya A, et al. Prediction of no-reflow and major adverse cardiovascular events with a new scoring system in STEMI patients. *J Interv Cardiol.* 2018;31(2):144–149. [CrossRef]
10. Esteva A, Chou K, Yeung S, et al. Deep learning-enabled medical computer vision. *NPJ Digit Med.* 2021;4(1):5. [CrossRef]
11. Rajkumar A, Dean J, Kohane I. Machine Learning in Medicine. *N Engl J Med.* 2019;380(14):1347–1358. [CrossRef]
12. Liu P, Li XJ, Zhang T, Huang YH. Comparison between XGboost model and logistic regression model for predicting sepsis after extremely severe burns. *J Int Med Res.* 2024;52(5):3000605241247696. [CrossRef]
13. Iyer K, Nallamothu BK, Figueroa CA, Nadakuditi RR. A multi-stage neural network approach for coronary 3D reconstruction from uncalibrated X-ray angiography images. *Sci Rep.* 2023;13(1):17603. [CrossRef]
14. Liu Z, Wang Y, Vaidya S, et al. Kan: Kolmogorov-arnold networks. *arXiv preprint.* April 30, 2024. doi: 10.48550/arXiv.2404.19756 [Epub ahead of print].
15. Erkan İ, Günen MA. Comparison of Zn recovery prediction from carbonate ores with machine-learning methods. *Int J Miner Metall Mater.* 2026;33:820–832. [CrossRef]
16. Lundberg SM, Lee SI. A unified approach to interpreting model predictions. *Adv Neural Inf Process Syst.* 2017;30:4765–4774.
17. Lin A, Kolossváry M, Motwani M, et al. Artificial Intelligence in Cardiovascular Imaging for Risk Stratification in Coronary Artery Disease. *Radiol Cardiothorac Imaging.* 2021;3(1):e200512. [CrossRef]
18. Wang H, Zu Q, Chen J, Yang Z, Ahmed MA. Application of Artificial Intelligence in Acute Coronary Syndrome: A Brief Literature Review. *Adv Ther.* 2021;38(10):5078–5086. [CrossRef]
19. Dong-bao L, Qi H, Zhi L, Shan W, Wei-ying J. Predictors and long-term prognosis of angiographic slow/no-reflow phenomenon during emergency percutaneous coronary intervention for ST-elevated acute myocardial infarction. *Clin Cardiol.* 2010;33(12):E7–E12. [CrossRef]
20. Wang L, Huang S, Zhou Q, Dou L, Lin D. The predictive value of laboratory parameters for no-reflow phenomenon in patients with ST-elevation myocardial infarction following primary percutaneous coronary intervention: A meta-analysis. *Clin Cardiol.* 2024;47(2):e24238. [CrossRef]
21. Khalaji A, Behnouth AH, Jameie M, et al. Machine learning algorithms for predicting mortality after coronary artery bypass grafting. *Front Cardiovasc Med.* 2022;9:977747. [CrossRef]
22. Kendale S, Kulkarni P, Rosenberg AD, Wang J. Supervised Machine-learning Predictive Analytics for Prediction of Postinduction Hypotension. *Anesthesiology.* 2018;129(4):675–688. [CrossRef]
23. Deng L, Zhao X, Su X, Zhou M, Huang D, Zeng X. Machine learning to predict no reflow and in-hospital mortality in patients with ST-segment elevation myocardial infarction that underwent primary percutaneous coronary intervention. *BMC Med Inform Decis Mak.* 2022;22(1):109. [CrossRef]
24. Celik T, Balta S, Demir M, et al. Predictive value of admission red cell distribution width–platelet ratio for no-reflow phenomenon in acute ST segment elevation myocardial infarction undergoing primary percutaneous coronary intervention. *Cardiol J.* 2016;23(1):84–92. [CrossRef]
25. Kurtul A, Yarlioglu M, Celik IE, et al. Association of lymphocyte-to-monocyte ratio with the no-reflow phenomenon in patients who underwent a primary percutaneous coronary intervention for ST-elevation myocardial infarction. *Coron Artery Dis.* 2015;26(8):706–712. [CrossRef]
26. Toprak K, Toprak İH, Acar O, Ermiş MF. The predictive value of the HALP score for no-reflow phenomenon and short-term mortality in patients with ST-elevation myocardial infarction. *Postgrad Med.* 2024;136(2):169–179. [CrossRef]